STABILITY ANALYSIS OF LARGE TIME-STEPPING METHODS FOR EPITAXIAL GROWTH MODELS*

CHUANJU XU† AND TAO TANG‡

Abstract. Numerical methods for solving the continuum model of the dynamics of the molecular beam epitaxy (MBE) require very large time simulation, and therefore large time steps become necessary. The main purpose of this work is to construct and analyze highly stable time discretizations which allow much larger time steps than those of a standard implicit-explicit approach. To this end, an extra term, which is consistent with the order of the time discretization, is added to stabilize the numerical schemes. Then the stability properties of the resulting schemes are established rigorously. Numerical experiments are carried out to support the theoretical claims. The proposed methods are also applied to simulate the MBE models with large solution times. The power laws for the coarsening process are obtained and are compared with previously published results.

1. Introduction. Recently there has been significant research interest in the dynamics of molecular beam epitaxy (MBE) growth. The MBE technique is among the most refined methods for the growth of thin solid films, and it is of great importance for applied studies; see, e.g., [1, 16, 22]. The evolution of the surface morphology during epitaxial growth results in a delicate relation between the molecular flux and the relaxation of the surface profile through surface diffusion of adatoms. It occurs on time and length scales that may span several orders of magnitude. Different kinds of models have been used to describe such phenomena; these typically include *atomistic models, continuum models, and hybrid models*. The atomistic models are usually implemented in the form of molecular dynamics or kinetic Monte Carlo simulations [4, 9, 17]. The continuum models are based on partial differential equations and are appropriate mainly for investigating the temporal evolution of the MBE instability at large time and length scales [11, 24]. The hybrid models can be considered as a compromise between atomistic models and continuum models; see, e.g., [3, 8].

We are interested in the continuum models for the evolution of the MBE growth. Let $h(\mathbf{x}, t)$ be the epitaxy surface height with $\mathbf{x} \in \mathbb{R}^2$ and $t \geq 0$. Under typical conditions for MBE growth, the height evolution equation can be written under mass conservation form (see, e.g., [14]):

$$(1.1) \qquad h_t = -\nabla \cdot J(\nabla h),$$

---

where J is the surface current which can be decomposed into a sum of two currents,

$$(1.2) \qquad\qquad J = J_{\mathrm{SD}} + J_{\mathrm{NE}},$$

where J_{SD} is the equilibrium surface current describing the surface diffusion and J_{NE} is the nonequilibrium diffusion current taking into account the Ehrlich–Schwoebel effect [6, 18]. The surface diffusion current has the form

$$(1.3) \qquad\qquad J_{\mathrm{SD}} = \delta \nabla(\Delta h),$$

where δ is the surface diffusion constant. By using effective free energy formulation, the nonequilibrium diffusion current under consideration can be written in the form

$$(1.4) \qquad\qquad J_{\mathrm{NE}}(M) = -\frac{\partial U(M)}{\partial M},$$

where $M = (M_1, M_2) := \nabla h$ is the slope vector and $U(M)$ is the potential depending only on the slope vector. Evidently, the term J_{NE} helps the system (1.1) to evolve toward the states in which the slope M attains the minimum of $U(M)$ because J_{NE} vanishes at the minima of $U(M)$. The minima of this potential is the preferred value of the slope. Consequently, the corresponding system is the so-called epitaxial growth model with slope selection.

The continuum model (1.1) has been extensively applied to modeling interfacial coarsening dynamics in epitaxial growth with slope selection; see, e.g., [12, 14, 24]. In (1.1), the fourth-order term models surface diffusion, and the nonlinear second-order term models the well-known Ehrlich–Schowoebel effect [6, 18], which gives rise to instabilities in the evolution of the surface morphology. The instability then leads to the formation of mounds and pyramids on the growing surface. These pyramid-like structures have been reported in many experiments and numerical simulations; see, e.g., [14, 20, 23]. It is found that the lateral width λ and the height w of these pyramids grow in time as power laws with the same component. Thus, the ratio w/λ, corresponding to the pyramid slope, approaches a constant at large times. Therefore, there is a slope selection in a typical MBE growth. The corresponding coarsening exponents were found from experiments to depend on the symmetry of the surface. Two typical values of the coarsening exponent have been found, namely 1/4 (see, e.g., [14, 20]) and 1/3 (see, e.g., [14, 23]). Some mathematical justification of such predictions was given in [10]. We also point out that the continuum model (1.1)–(1.4) has been derived by Ortiz, Repetto, and Si [15] by using a series expansion of the deposition flux in powers of the surface gradient. They also provided an explicit construction for the pyramid-like coarsening, which allows one to predict characteristic power laws for the pyramid size growth. However, it is difficult to provide growing details, especially for complex thin-film systems.

Numerical simulations with the continuum models are appropriate for investigating the surface growth instability at large times. The direct numerical simulation for (1.1)–(1.4) with different nonequilibrium diffusion currents was performed by Siegert [19], who obtained a power law close to 1/4. Moldovan and Golubovic [14] carried out very comprehensive numerical simulations by using a kinetic scaling theory and obtained a 1/3 power law. It should be pointed out that the simulations reported in [14] were not completely based on a continuum model. Instead, they solved a so-called type-A dynamics equation directly on a hexagonal grid. More recently, the well-posedness of the initial-boundary-value problem of (1.1) is studied by Li and Liu [12]

using the perturbation analysis and Galerkin spectral approximations. In [13], they used variational techniques to obtain some asymptotic results for a no-slope-selection model. Moreover, several scaling laws have been derived in [13].

The main purpose of this study is to provide efficient numerical schemes for solving (1.1), with particular emphasis on the use of large time steps. To obtain meaningful results for power laws, the integration times in simulations have to be very large (say, in the order of 10^4). As a result, it is reasonable to employ larger time steps and a small number of grid points in computations, provided that stability and accuracy can be preserved. It is observed that most of the existing continuum model simulations have used an explicit integration method in time and finite difference type approximation in space. To maintain the stability and to achieve high approximation accuracy, the number of spatial grid points must be large and the time step has to be small. Even with rapidly increasing computational resources, explicit schemes are still limited to simulating early surface evolution and therefore small length scale [12].

The main objectives of this work are threefold: First, we introduce an accurate and efficient semi-implicit Fourier pseudospectral method for solving the time-dependent nonlinear diffusion equations (1.1). To approximate the time derivatives, a backward differentiation is employed. More precisely, the fourth-order term is treated implicitly to reduce the associated stability constraints, while the nonlinear second-order terms are treated explicitly in order to avoid solving the nonlinear equations at each time step. Secondly, a stabilization second-order term is added to the discretized system, which increases the time step dramatically. In real applications, the surface diffusion constant δ may be very small after dimensional scaling. Consequently, direct use of the standard semi-implicit method still suffers from severe stability restriction on the time step. In order to overcome this difficulty, we introduce a stabilization term with constant coefficient A, which allows us to increase the time step significantly. Note that a similar technique has been used by Zhu et al. in the simulation of the Cahn–Hilliard equation [26]. Our main contribution is to show rigorously that the resulting numerical scheme is stable if an appropriate constant A is chosen. Justification of this stabilization technique is provided by considering several numerical tests. Finally, we perform some numerical simulations for the interfacial coarsening dynamics using our proposed schemes. Our numerical results yield a 1/3 power law for the isotropic symmetry surface and 1/4 for the square symmetry surface.

It is worthwhile to mention some recent papers by Feng and Prohl on the numerical analysis for Cahn–Hilliard and Allen–Cahn equations; see, e.g., [7]. They also studied stability issues—the continuous dependence of solutions on the initial data. This is different from our stability concept, which seems more related to the decay of energy. They mainly proved that the stability constant increases to infinity algebraically as a small parameter (similar to our surface diffusion constant δ in (1.3)) goes to 0. This is a big step forward, since usually the blow-up of the constant is exponential if one uses the Gronwall inequality—a standard method.

The organization of the paper is as follows. In section 2, we construct highly stable semi-implicit Fourier spectral methods for solving (1.1), which is of first-order accuracy in time. To improve the numerical stability, an $\mathcal{O}(\Delta t)$ term is added. Detailed stability analysis based on the energy method is provided to show that the proposed methods allow a large time step, and therefore are useful for large time simulations. The second-order semi-implicit methods are investigated in section 3. It will be demonstrated that the stability analysis for higher-order time-stepping methods is much more difficult. Numerical experiments for model problems are presented in

section 4. Section 5 reports some computational results for the coarsening dynamics using the numerical schemes allowing large time steps. Some concluding remarks are given in the final section.

2. Semi-implicit time discretization: First-order methods. To demonstrate the main ideas in scheme designing and stability analysis, we will use two model equations in this work. The first one is of the form

$$(2.1) \qquad h_t = -\delta \Delta^2 h - \nabla \cdot [(1 - |\nabla h|^2)\nabla h], \quad (\mathbf{x}, t) \in \Omega \times (0, T].$$

The second model equation is of the form

$$(2.2) \qquad h_t = -\delta \Delta^2 h - ((1 - |h_x|^2)h_x)_x - ((1 - |h_y|^2)h_y)_y, \quad (\mathbf{x}, t) \in \Omega \times (0, T].$$

Hereafter, we use h_t to denote $\frac{\partial h}{\partial t}$, $\nabla h = (h_x, h_y)$. Both model problems are subject to the periodic boundary conditions and suitable initial data, where $\Omega = (0, L)^2$ with $L > 0$. The model (2.1) corresponds to the isotropic surface current, while (2.2) represents the simplest square surface current.

For the MBE simulations, large computational domain is necessary in order to minimize the effect of periodicity assumption and to collect enough statistical information such as mean surface height and width of the pyramid-like structures. Moreover, sufficiently long integration time is necessary in order to detect the epitaxy growth behaviors and to reach the physical scaling regime. On the other hand, to carry out numerical simulations with large time and large computational domain, highly stable and accurate numerical methods are required. To this end, it is natural to use the Fourier spectral approach in space which has been found extremely efficient for periodic problems. As for stability issue, the implicit treatment for the fourth-order terms is employed, and more importantly, a special trick to handle the nonlinear second-order terms is used. The goal is to significantly increase the allowed time steps.

We first consider the MBE model with the isotropic symmetry current, namely, (2.1). A classical first-order semi-implicit scheme is of the form

$$(2.3) \qquad \frac{h^{n+1} - h^n}{\Delta t} + \delta \Delta^2 h^{n+1} = -\nabla \cdot \left[(1 - |\nabla h^n|^2)\nabla h^n \right], \ \ n \geq 0.$$

It is expected that the implicit treatment for the fourth-order term in (2.3) allows one to relax the time step restriction. However, numerical experiments demonstrate that a larger time step cannot be used for the scheme (2.3) when δ is small; see, e.g., [12]. To improve this, an $\mathcal{O}(\Delta t)$ term is added into the scheme (2.3):

$$(2.4) \quad \frac{h^{n+1} - h^n}{\Delta t} + \delta \Delta^2 h^{n+1} - A\Delta h^{n+1} = -\nabla \cdot \left[(1 - |\nabla h^n|^2 + A)\nabla h^n \right], \ \ n \geq 0,$$

where A is a positive constant to be determined later and $h^n \equiv h^n(\mathbf{x})$ is an approximation of $h(\mathbf{x}, t)$ at $t = t^n$. The initial data h^0 is given by the initial condition. The purpose for adding the extra terms is to improve the stability condition so that larger time steps can be used. This will be justified theoretically in this section, and will be demonstrated by our numerical results in section 4.

In order to study its stability property, we will use a discrete energy estimate. To this end, we first state the following known result.

LEMMA 2.1 (energy identities [12]). *If $h(\mathbf{x}, t)$ is a solution of (2.1), then the following energy identities hold:*

$$(2.5) \qquad \frac{d}{dt}\|h\|^2 + 4E(h) + \|\nabla h\|_{L^4}^4 = |\Omega|,$$

$$(2.6) \qquad \frac{d}{dt}E(h) + \|h_t\|^2 = 0,$$

where $\|\cdot\|$ is the standard L^2-norm in Ω, L^p is the standard L^p-norm, and

$$(2.7) \qquad E(h) = \int_\Omega \left[\frac{1}{4}(|\nabla h|^2 - 1)^2 + \frac{\delta}{2}|\Delta h|^2\right] d\mathbf{x}.$$

We briefly sketch the proof of (2.5) and (2.6), which is useful in deriving its discrete counterparts. It follows from (2.1) that

$$\langle h_t,\, \varphi \rangle = -\left\langle \nabla \cdot [(1 - |\nabla h|^2)\nabla h + \delta\nabla\Delta h],\, \varphi \right\rangle,$$

where $\langle \cdot, \cdot \rangle$ denotes the standard inner product in the L^2-space. It can be verified directly that setting $\varphi = h$ gives (2.5) and setting $\varphi = h_t$ yields (2.6).

THEOREM 2.1. *If the constant A in (2.4) is sufficiently large, then the following energy inequality holds:*

$$(2.8) \qquad E(h^{n+1}) \le E(h^n),$$

where E is defined by (2.7) and h^n is computed by (2.4). Moreover, if the numerical solution is convergent in $L^\infty([0, T]; W^{1,\infty}(\Omega))$ as $\Delta t \to 0$, then the constant A can be chosen to satisfy

$$(2.9) \qquad A \ge \frac{3}{2}|\nabla h|^2 - \frac{1}{2} \qquad \textit{a.e. in } \Omega \times (0, T],$$

where $h(\mathbf{x}, t)$ is a solution of (2.1).

Proof. For any L-periodic $H^2(\Omega)$ function φ, it follows from (2.4) that

$$(2.10) \quad \frac{1}{\Delta t}\left\langle h^{n+1} - h^n,\, \varphi \right\rangle + \delta\left\langle \Delta h^{n+1}, \Delta\varphi \right\rangle + A\left\langle \nabla(h^{n+1} - h^n), \nabla\varphi \right\rangle + I(\varphi) = 0,$$

where

$$I(\varphi) := \left\langle (|\nabla h^n|^2 - 1)\nabla h^n,\, \nabla\varphi \right\rangle.$$

Letting $\varphi = \delta_t h^n := h^{n+1} - h^n$ gives

$$(2.11) \qquad \frac{1}{\Delta t}\|\delta_t h^n\|^2 + \delta\left\langle \Delta h^{n+1}, \Delta\delta_t h^n \right\rangle + A\left\langle \nabla\delta_t h^n, \nabla\delta_t h^n \right\rangle + I(\delta_t h^n) = 0.$$

Observe that

$$
\begin{aligned}
I(\delta_t h^n) &= \left\langle |\nabla h^n|^2 - 1, \nabla h^n \cdot \nabla h^{n+1} - |\nabla h^n|^2 \right\rangle \\
&= \left\langle |\nabla h^n|^2 - 1, -\frac{1}{2}|\nabla\delta_t h^n|^2 + \frac{1}{2}|\nabla h^{n+1}|^2 - \frac{1}{2}|\nabla h^n|^2 \right\rangle \\
&= -\frac{1}{2}\left\langle |\nabla h^n|^2 - 1, |\nabla\delta_t h^n|^2 \right\rangle + \frac{1}{2}\left\langle (|\nabla h^n|^2 - 1)(|\nabla h^{n+1}|^2 - |\nabla h^n|^2), 1 \right\rangle \\
&= -\frac{1}{2}\left\langle |\nabla h^n|^2 - 1, |\nabla\delta_t h^n|^2 \right\rangle + \frac{1}{2}\left\langle |\nabla h^n|^2 \cdot |\nabla h^{n+1}|^2, 1 \right\rangle \\
&\quad + \frac{1}{2}\left\langle -|\nabla h^n|^4 - |\nabla h^{n+1}|^2 + |\nabla h^n|^2, 1 \right\rangle.
\end{aligned}
$$

Using the identity $2a^2b^2 = -(a^2 - b^2)^2 + a^4 + b^4$ to the second last term above with $a = |\nabla h^{n+1}|$ and $b = |\nabla h^n|$, we obtain

$$
\begin{aligned}
I(\delta_t h^n) = &-\frac{1}{2}\left\langle|\nabla h^n|^2 - 1, |\nabla\delta_t h^n|^2\right\rangle - \frac{1}{4}\left\langle(|\nabla h^{n+1}|^2 - |\nabla h^n|^2)^2, 1\right\rangle \\
&+\frac{1}{4}\left\langle|\nabla h^{n+1}|^4 + |\nabla h^n|^4, 1\right\rangle + \frac{1}{2}\left\langle-|\nabla h^n|^4 - |\nabla h^{n+1}|^2 + |\nabla h^n|^2, 1\right\rangle \\
= &\left\langle-\frac{1}{2}(|\nabla h^n|^2 - 1) - \frac{1}{4}|\nabla h^{n+1} + \nabla h^n|^2, |\nabla\delta_t h^n|^2\right\rangle \\
&+\frac{1}{4}\left\langle|\nabla h^{n+1}|^4 - |\nabla h^n|^4 - 2|\nabla h^{n+1}|^2 + 2|\nabla h^n|^2, 1\right\rangle
\end{aligned}
$$

$$
\begin{aligned}
(2.12) \qquad = &\left\langle-\frac{1}{2}(|\nabla h^n|^2 - 1) - \frac{1}{4}|\nabla h^{n+1} + \nabla h^n|^2, |\nabla\delta_t h^n|^2\right\rangle \\
&+\frac{1}{4}\left(\||\nabla h^{n+1}|^2 - 1\|^2 - \||\nabla h^n|^2 - 1\|^2\right).
\end{aligned}
$$

Combining (2.11) and (2.12) yields

$$
\begin{aligned}
(2.13) \quad &\frac{1}{\Delta t}\|\delta_t h^n\|^2 + \delta\left\langle\Delta h^{n+1}, \Delta\delta_t h^n\right\rangle + \frac{1}{4}\left(\||\nabla h^{n+1}|^2 - 1\|^2 - \||\nabla h^n|^2 - 1\|^2\right) \\
&+\left\langle A - \frac{1}{2}(|\nabla h^n|^2 - 1) - \frac{1}{4}|\nabla h^{n+1} + \nabla h^n|^2, |\delta_t h^n|^2\right\rangle = 0.
\end{aligned}
$$

Note that the last term in (2.13) can be made nonnegative provided that

$$
(2.14) \qquad\qquad A \geq \max_{\mathbf{x}\in\Omega}\left\{\frac{1}{2}(|\nabla h^n|^2 - 1) + \frac{1}{4}|\nabla h^{n+1} + \nabla h^n|^2\right\}.
$$

Observe that

$$
\begin{aligned}
(2.15) \qquad\qquad \delta\left\langle\Delta h^{n+1}, \Delta\delta_t h^n\right\rangle &= \delta\left\langle\Delta h^{n+1}, \Delta h^{n+1} - \Delta h^n\right\rangle \\
&\geq \frac{\delta}{2}\|\Delta h^{n+1}\|^2 - \frac{\delta}{2}\|\Delta h^n\|^2.
\end{aligned}
$$

Consequently, Theorem 2.1 follows from (2.13)–(2.15).   □

We now consider the MBE model with the square symmetric surface (2.2). An energy equality similar to that for the model (2.1) can be established.

LEMMA 2.2. *If $h(\mathbf{x}, t)$ is a solution of (2.2), then the following energy equalities hold:*

$$
(2.16) \qquad\qquad \frac{d}{dt}E_2(h) + \|h_t\|^2 = 0,
$$

$$
(2.17) \qquad\qquad \frac{d}{dt}\|h\|^2 + 4E_2(h) + \|h_x\|_{L^4}^4 + \|h_y\|_{L^4}^4 = 2|\Omega|,
$$

where

$$
(2.18) \qquad E_2(h) = \int_\Omega \left\{\frac{\delta}{2}|\Delta h|^2 + \frac{1}{4}\left[(h_x^2 - 1)^2 + (h_y^2 - 1)^2\right]\right\} d\mathbf{x}.
$$

Proof. Equation (2.2) is equivalent to

$$
(2.19) \qquad\qquad h_t + \delta\Delta^2 h = -\nabla \cdot J,
$$

where $J = (J_1, J_2)$ is given by

$$J_1 = \left(1 - h_x^2\right) h_x, \qquad J_2 = (1 - h_y^2) h_y.$$

Multiplying both sides of (2.19) with h_t gives

(2.20)
$$\|h_t\|^2 + \delta \langle \Delta h, (\Delta h)_t \rangle = \langle J, (\nabla h)_t \rangle.$$

Observe

$$\langle J, (\nabla h)_t \rangle = \left\langle (1 - h_x^2) h_x, h_{xt} \right\rangle + \left\langle (1 - h_y^2) h_y, h_{yt} \right\rangle$$
$$= -\frac{1}{4} \frac{d}{dt} \int_\Omega \left[(h_x^2 - 1)^2 + (h_y^2 - 1)^2 \right] d\mathbf{x}.$$

The above result and (2.20) yield (2.16). Similarly, the energy equality (2.17) can be derived by multiplying (2.19) with h.   □

Similar to the scheme (2.4), a first-order scheme is constructed for the MBE model (2.2):

(2.21)
$$\frac{h^{n+1} - h^n}{\Delta t} + \delta \Delta^2 h^{n+1} - A \Delta h^{n+1}$$
$$= -A \Delta h^n - \left[(1 - (h_x^n)^2) h_x^n \right]_x - \left[(1 - (h_y^n)^2) h_y^n \right]_y.$$

THEOREM 2.2. *If A in (2.21) is chosen sufficiently large, then the following energy inequality holds:*

(2.22)
$$E_2(h^{n+1}) \le E_2(h^n),$$

where E_2 is defined by (2.18) and h^n is computed by (2.21). Moreover, if the numerical solution of (2.21) is convergent, then A can be chosen to satisfy

(2.23)
$$A \ge \max \left\{ \frac{3}{2} h_x^2 - \frac{1}{2}, \ \frac{3}{2} h_y^2 - \frac{1}{2} \right\} \qquad a.e. \ in \ \Omega \times (0, T],$$

where $h(\mathbf{x}, t)$ is the solution of (2.2).

Proof. The proof follows in the same manner as that of Theorem 2.1. By direct computations, we can obtain

$$\frac{1}{\Delta t} \|\delta_t h^n\|^2 + E_2(h^{n+1}) - E_2(h^n)$$
$$+ \int \left[A - \frac{1}{2} \left((h_x^n)^2 - 1 \right) - \frac{1}{4} (h_x^{n+1} + h_x^n)^2 \right] (h_x^{n+1} - h_x^n)^2 \, d\mathbf{x}$$
$$+ \int \left[A - \frac{1}{2} \left((h_y^n)^2 - 1 \right) - \frac{1}{4} (h_y^{n+1} + h_y^n)^2 \right] (h_y^{n+1} - h_y^n)^2 \, d\mathbf{x} = 0.$$

It follows from the above result that (2.22) holds provided that

$$A \ge \max_{\mathbf{x} \in \Omega} \left\{ \frac{1}{2} \left((h_x^n)^2 - 1 \right) - \frac{1}{4} \left(h_x^{n+1} + h_x^n \right)^2 \right\}$$

and

$$A \ge \max_{\mathbf{x} \in \Omega} \left\{ \frac{1}{2} \left((h_y^n)^2 - 1 \right) - \frac{1}{4} \left(h_y^{n+1} + h_y^n \right)^2 \right\}.$$

If the numerical solution is convergent, then the above conditions become inequality (2.23).   □

3. Semi-implicit time discretization: Higher-order methods.

3.1. Second-order scheme: BD2/EP2. By combining a second-order backward differentiation (BD2) for the time derivative term and a second-order extrapolation (EP2) for the explicit treatment of the nonlinear term, we arrive at a second-order scheme (BD2/EP2) for (2.1):

(3.1)
$$\frac{3h^{n+1} - 4h^n + h^{n-1}}{2\Delta t} + \delta\Delta^2 h^{n+1} - A\Delta h^{n+1}$$
$$= -2A\Delta h^n + A\Delta h^{n-1} - \nabla \cdot [(1 - |\nabla(2h^n - h^{n-1})|^2)\nabla(2h^n - h^{n-1})] \quad \forall n \geq 1.$$

As usual, to start the iteration $h^0(\mathbf{x})$ is given by the initial condition, and $h^1(\mathbf{x})$ is computed by the first-order scheme (2.4).

THEOREM 3.1. *If the constant A in* (3.1) *is sufficiently large, then the following energy inequality holds:*

(3.2)
$$\widetilde{E}^{n+1} \leq \widetilde{E}^n + \mathcal{O}(\Delta t^2),$$

where $\widetilde{E}^n$ is defined by

(3.3) $\widetilde{E}^n = \frac{1}{\Delta t}\|h^n - h^{n-1}\|^2 + \frac{1}{4}\left\||\nabla h^n|^2 - 1\right\|^2 + \frac{\delta}{2}\|\Delta h^n\|^2 + \frac{A}{2}\|\nabla(h^n - h^{n-1})\|^2.$

In particular, we can obtain

(3.4)
$$E(h^n) \leq E(h^1) + \mathcal{O}(\Delta t),$$

where E is defined by (2.7). *Moreover, if the numerical solution of* (3.1) *is convergent in $L^\infty([0,T]; W^{1,\infty}(\Omega))$ as $\Delta t \to 0$, then the constant A can be chosen to satisfy*

(3.5)
$$A \geq 3|\nabla h|^2 - 1 \quad a.e. \ in \ \Omega \times (0,T],$$

where $h(x,t)$ is a solution of (2.1).

Proof. For ease of notation, let $\delta_t h^n = h^{n+1} - h^n$ and $\delta_{tt} h^n = h^{n+1} - 2h^n + h^{n-1}$. Multiplying both sides of (3.1) by $\delta_t h^n$ and integrating the resulting equation in Ω give

(3.6)
$$I_1^n + I_2^n + I_3^n = I_4^n,$$

where

$$I_1^n := \frac{1}{2\Delta t}\langle 3\delta_t h^n - \delta_t h^{n-1}, \delta_t h^n\rangle,$$
$$I_2^n := \delta\langle \Delta^2 h^{n+1}, \delta_t h^n\rangle,$$
$$I_3^n := -A\langle \Delta\delta_{tt} h^n, \delta_t h^n\rangle,$$
$$I_4^n := -\langle \nabla \cdot [(1 - |\nabla(2h^n - h^{n-1})|^2)\nabla(2h^n - h^{n-1})], \delta_t h^n\rangle.$$

We now estimate them term by term. The estimate for the first three terms is straightforward:

(3.7) $\quad I_1^n \geq \frac{5}{4\Delta t}\|\delta_t h^n\|^2 - \frac{1}{4\Delta t}\|\delta_t h^{n-1}\|^2 \geq \frac{1}{\Delta t}\|\delta_t h^n\|^2 - \frac{1}{\Delta t}\|\delta_t h^{n-1}\|^2,$

(3.8) $\quad I_2^n = \delta\langle \Delta h^{n+1}, \Delta h^{n+1} - \Delta h^n\rangle \geq \frac{\delta}{2}\|\Delta h^{n+1}\|^2 - \frac{\delta}{2}\|\Delta h^n\|^2,$

(3.9) $\quad I_3^n = A\langle \delta_{tt}\nabla h^n, \delta_t\nabla h^n\rangle = A\langle \delta_t\nabla h^n - \delta_t\nabla h^{n-1}, \delta_t\nabla h^n\rangle$
$$= \frac{A}{2}\|\delta_t\nabla h^n\|^2 - \frac{A}{2}\|\delta_t\nabla h^{n-1}\|^2 + \frac{A}{2}\|\delta_{tt}\nabla h^n\|^2.$$

To estimate I_4^n, we need the following two identities. On one hand, we have

(3.10)
$$\begin{aligned}
&\nabla(2h^n - h^{n-1}) \cdot \nabla(h^{n+1} - h^n) \\
&= \nabla(2h^n - h^{n-1}) \cdot \nabla h^{n+1} - \nabla(2h^n - h^{n-1}) \cdot \nabla h^n \\
&= -\frac{1}{2}|\delta_{tt}\nabla h^n|^2 + \frac{1}{2}|\nabla(2h^n - h^{n-1})|^2 + \frac{1}{2}|\nabla h^{n+1}|^2 - \nabla(2h^n - h^{n-1}) \cdot \nabla h^n,
\end{aligned}$$

and on the other hand,

(3.11)
$$\begin{aligned}
&\nabla(2h^n - h^{n-1}) \cdot \nabla(h^{n+1} - h^n) = \nabla h^n \cdot \nabla(h^{n+1} - h^n) + \delta_t \nabla h^n \cdot \delta_t \nabla h^{n-1} \\
&= \frac{1}{2}|\nabla h^{n+1}|^2 - \frac{1}{2}|\nabla h^n|^2 - \frac{1}{2}|\delta_t \nabla h^n|^2 - \frac{1}{2}|\delta_{tt}\nabla h^n|^2 + \frac{1}{2}|\delta_t \nabla h^n|^2 + \frac{1}{2}|\delta_t \nabla h^{n-1}|^2 \\
&= \frac{1}{2}|\nabla h^{n+1}|^2 - \frac{1}{2}|\nabla h^n|^2 - \frac{1}{2}|\delta_{tt}\nabla h^n|^2 + \frac{1}{2}|\delta_t \nabla h^{n-1}|^2.
\end{aligned}$$

Using (3.10) gives

(3.12)
$$\begin{aligned}
&\left\langle -|\nabla(2h^n - h^{n-1})|^2 \nabla(2h^n - h^{n-1}), \nabla(h^{n+1} - h^n) \right\rangle \\
&= \frac{1}{2}\left\langle |\nabla(2h^n - h^{n-1})|^2, |\delta_{tt}\nabla h^n|^2 \right\rangle + J_4^n,
\end{aligned}$$

where

$$\begin{aligned}
J_4^n &:= \left\langle -|\nabla(2h^n - h^{n-1})|^2, \frac{1}{2}|\nabla(2h^n - h^{n-1})|^2 + \frac{1}{2}|\nabla h^{n+1}|^2 - \nabla(2h^n - h^{n-1}) \cdot \nabla h^n \right\rangle \\
&= \frac{1}{2}\left\langle 1, -|\nabla(2h^n - h^{n-1})|^4 \right\rangle + \frac{1}{2}\left\langle -|\nabla(2h^n - h^{n-1})|^2, |\nabla h^{n+1}|^2 \right\rangle \\
&\quad + \left\langle |\nabla(2h^n - h^{n-1})|^2, \nabla(2h^n - h^{n-1}) \cdot \nabla h^n \right\rangle \\
&= -\frac{3}{4}\left\langle 1, |\nabla(2h^n - h^{n-1})|^4 \right\rangle + \frac{1}{4}\||\nabla(2h^n - h^{n-1})|^2 - |\nabla h^{n+1}|^2\|^2 \\
&\quad - \frac{1}{4}\left\langle 1, |\nabla h^{n+1}|^4 \right\rangle + \left\langle |\nabla(2h^n - h^{n-1})|^2, \nabla(2h^n - h^{n-1}) \cdot \nabla h^n \right\rangle.
\end{aligned}$$

Using the Schwartz inequality to the last term above gives

$$\begin{aligned}
&\left\langle |\nabla(2h^n - h^{n-1})|^2, \nabla(2h^n - h^{n-1}) \cdot \nabla h^n \right\rangle \\
&\leq \frac{1}{2}\left\langle |\nabla(2h^n - h^{n-1})|^2, |\nabla(2h^n - h^{n-1})|^2 \right\rangle + \frac{1}{2}\left\langle |\nabla(2h^n - h^{n-1})|^2, |\nabla h^n|^2 \right\rangle \\
&\leq \frac{1}{2}\left\langle 1, |\nabla(2h^n - h^{n-1})|^4 \right\rangle + \frac{1}{4}\left\langle 1, |\nabla(2h^n - h^{n-1})|^4 \right\rangle + \frac{1}{4}\left\langle 1, |\nabla h^n|^4 \right\rangle \\
&= \frac{3}{4}\left\langle 1, |\nabla(2h^n - h^{n-1})|^4 \right\rangle + \frac{1}{4}\left\langle 1, |\nabla h^n|^4 \right\rangle.
\end{aligned}$$

Combining the above two results gives

(3.13)
$$\begin{aligned}
J_4^n &\leq \frac{1}{4}\||\nabla(2h^n - h^{n-1})|^2 - |\nabla h^{n+1}|^2\|^2 - \frac{1}{4}\left\langle 1, |\nabla h^{n+1}|^4 \right\rangle + \frac{1}{4}\left\langle 1, |\nabla h^n|^4 \right\rangle \\
&= \frac{1}{4}\left\langle |\nabla(h^{n+1} + 2h^n - h^{n-1})|^2, |\delta_{tt}\nabla h^n|^2 \right\rangle - \frac{1}{4}\left\langle 1, |\nabla h^{n+1}|^4 \right\rangle + \frac{1}{4}\left\langle 1, |\nabla h^n|^4 \right\rangle.
\end{aligned}$$

Using the definition of I_4^n, together with (3.11), (3.12), and (3.13), we have

$$I_4^n = \left\langle (1 - |\nabla(2h^n - h^{n-1})|^2)\nabla(2h^n - h^{n-1}),\, \nabla(h^{n+1} - h^n) \right\rangle$$

$$= \frac{1}{2}\|\nabla h^{n+1}\|^2 - \frac{1}{2}\|\nabla h^n\|^2 - \frac{1}{2}\|\delta_{tt}\nabla h^n\|^2 + \frac{1}{2}\|\delta_t\nabla h^{n-1}\|^2$$

$$+ \frac{1}{2}\left\langle |\nabla(2h^n - h^{n-1})|^2,\, |\delta_{tt}\nabla h^n|^2 \right\rangle + J_4^n$$

$$\leq -\frac{1}{2}\left\langle 1 - |\nabla(2h^n - h^{n-1})|^2,\, |\delta_{tt}\nabla h^n|^2 \right\rangle + \frac{1}{2}\|\nabla h^{n+1}\|^2 - \frac{1}{2}\|\nabla h^n\|^2 + \frac{1}{2}\|\delta_t\nabla h^{n-1}\|^2$$

$$+ \frac{1}{4}\left\langle |\nabla(h^{n+1} + 2h^n - h^{n-1})|^2,\, |\delta_{tt}\nabla h^n|^2 \right\rangle - \frac{1}{4}\left\langle 1, |\nabla h^{n+1}|^4 \right\rangle + \frac{1}{4}\left\langle 1, |\nabla h^n|^4 \right\rangle$$

$$= \left\langle \frac{1}{2}|\nabla(2h^n - h^{n-1})|^2 - \frac{1}{2} + \frac{1}{4}|\nabla(h^{n+1} + 2h^n - h^{n-1})|^2,\, |\delta_{tt}\nabla h^n|^2 \right\rangle$$

$$- \frac{1}{4}\||\nabla h^{n+1}|^2 - 1\|^2 + \frac{1}{4}\||\nabla h^n|^2 - 1\|^2 + \frac{1}{2}\|\delta_t\nabla h^{n-1}\|^2.$$

The above result, together with (3.6) and (3.7)–(3.9), yields

$$\widetilde{E}^{n+1} \leq \widetilde{E}^n + \frac{1}{2}\|\delta_t\nabla h^{n-1}\|^2$$

$$+ \left\langle -\frac{A}{2} + \frac{1}{2}|\nabla(2h^n - h^{n-1})|^2 - \frac{1}{2} + \frac{1}{4}|\nabla(h^{n+1} + 2h^n - h^{n-1})|^2,\, |\delta_{tt}\nabla h^n|^2 \right\rangle.$$

The last term above can be made nonpositive provided that

$$A \geq |\nabla(2h^n - h^{n-1})|^2 - 1 + \frac{1}{2}|\nabla(h^{n+1} + 2h^n - h^{n-1})|^2 \qquad \text{a.e. in } \Omega.$$

Using the fact that

$$\|\delta_t\nabla h^{n-1}\|^2 = \Delta t^2\|\nabla(h^n - h^{n-1})/\Delta t\|^2 = \mathcal{O}(\Delta t^2),$$

we obtain (3.2). Summing (3.2) over n gives $\widetilde{E}^n \leq \widetilde{E}^1 + \mathcal{O}(\Delta t)$. In particular, by using the definition of $\widetilde{E}$ and the energy E defined by (2.7), we have

$$E(h^n) \leq E(h^1) + \mathcal{O}(1)\Delta t,$$

where the $\mathcal{O}(1)$ term is given by

$$\mathcal{O}(1) = \|(h^1 - h^0)/\Delta t\|^2 + \frac{A}{2}\Delta t\|\nabla(h^1 - h^0)/\Delta t\|^2$$

$$+ \sum_{i=1}^{n-1} \Delta t\|\nabla(h^i - h^{i-1})/\Delta t\|^2.$$

This completes the proof of this theorem.   □

Remark 3.1. By comparing (2.9) and (3.5), we notice that the constant A used for the second-order scheme is two times larger than that for the first-order scheme.

Similarly, a second-order scheme of the BD2/EP2-type can be constructed for the square symmetry current model (2.2):

$$(3.14) \qquad \frac{3h^{n+1} - 4h^n + h^{n-1}}{2\Delta t} + \delta\Delta^2 h^{n+1} - A\Delta h^{n+1}$$

$$= -2A\Delta h^n + A\Delta h^{n-1} - \left[\left(1 - (2h_x^n - h_x^{n-1})^2\right)(2h_x^n - h_x^{n-1}) \right]_x$$

$$- \left[\left(1 - (2h_y^n - h_y^{n-1})^2\right)(2h_y^n - h_y^{n-1}) \right]_y.$$

Then an analysis similar to that of Theorem 3.1 can be carried out to obtain a stability result. The details will be omitted here.

3.2. Third-order scheme: BD3/EP3. A third-order scheme for solving the MBE model of general form (1.1) can be constructed in a similar manner as used in the last subsection. Specifically, we can obtain the BD3/EP3 scheme in the following form:

$$
(3.15) \quad
\begin{aligned}
&\frac{11h^{n+1} - 18h^n + 9h^{n-1} - 2h^{n-2}}{6\Delta t} + \delta\Delta^2 h^{n+1} - A\Delta h^{n+1} \\
&= -A\Delta(3h^n - 3h^{n-1} + h^{n-2}) - \nabla \cdot J(\nabla(3h^n - 3h^{n-1} + h^{n-2})) \quad \forall n \geq 2,
\end{aligned}
$$

where, in order to start the iteration, h^1, h^2 are calculated via a first- and second-order scheme, respectively.

The stability analysis of the scheme (3.15) requires some very detailed energy estimates and will not be presented here. The numerical results obtained in the next two sections indicate that the third-order time discretization of type (3.15) is also stable as long as the constant A is sufficiently large.

4. Numerical experiments: Stability and accuracy tests. A complete numerical algorithm also requires a discretization strategy in space. Since the Fourier spectral method is one of the most suitable spatial approximation methods for periodic problems [2, 5, 21, 25], it will be employed to handle the spatial discretization. To demonstrate the principal ideas, we consider the full discretization for the MBE model with the isotropic current using the first-order time-stepping method, namely, we will consider only the full discretization for (2.4). It is to find an approximate solution $h_K^n(\mathbf{x})$ in form of a truncated Fourier expansion:

$$
h_K^n(\mathbf{x}) = \sum_{k_1,k_2=-K}^{K} \hat{h}_{\mathbf{k}}^n \exp(-i\mathbf{k}\mathbf{x}),
$$

where $\mathbf{k} = (k_1, k_2)$ and K is a positive integer. The above expansion is required to satisfy the following weak formulation:

$$
(4.1) \quad
\begin{aligned}
&\frac{1}{\Delta t}\left\langle h_K^{n+1} - h_K^n, \varphi \right\rangle + \delta\left\langle \Delta h_K^{n+1}, \Delta\varphi \right\rangle + A\left\langle \nabla h_K^{n+1}, \nabla\varphi \right\rangle \\
&= \left\langle (1 - |\nabla h_K^n|^2 + A)\nabla h_K^n, \nabla\varphi \right\rangle \quad \forall \varphi \in S_K,
\end{aligned}
$$

where

$$
S_K = \text{span}\{\exp(-i\mathbf{k}\mathbf{x}), \quad -K \leq k_1, k_2 \leq K\}.
$$

For the full discretization problem (4.1), an energy inequality similar to that of Theorem 2.1 can be derived (its proof will be omitted here).

THEOREM 4.1. *Consider the numerical scheme* (4.1). *If*

$$
(4.2) \quad A \geq \max_{\mathbf{x}\in\Omega}\left\{\frac{1}{2}(|\nabla h_K^n|^2 - 1) + \frac{1}{4}|\nabla h_K^{n+1} + \nabla h_K^n|^2\right\},
$$

then the solution of (4.1) *satisfies*

$$
(4.3) \quad E(h_K^{n+1}) \leq E(h_K^n) \quad \forall n \geq 0,
$$

where the energy E is defined by (2.7). *Moreover, if the numerical solution of* (4.1) *is convergent in* $L^\infty([0,T]; W^{1,\infty}(\Omega))$ *as* $K \to \infty$ *and* $\Delta t \to 0$, *then the constant A can be chosen to satisfy*

$$(4.4) \qquad A \geq \frac{3}{2}|\nabla h|^2 - \frac{1}{2} \qquad a.e. \ in \ \Omega \times (0,T],$$

where $h(\mathbf{x},t)$ is a solution of (2.1).

By applying the Fourier transformation to (2.4), we obtain a set of ordinary differential equations for each mode $\mathbf{k}$ in the Fourier space,

$$(4.5) \qquad \frac{\hat{h}_{\mathbf{k}}^{n+1} - \hat{h}_{\mathbf{k}}^n}{\Delta t} + \delta|\mathbf{k}|^4 \hat{h}_{\mathbf{k}}^{n+1} + A|\mathbf{k}|^2 \hat{h}_{\mathbf{k}}^{n+1} = -i\mathbf{k} \left\{ (1 - |\nabla h_K^n|^2 + A)\nabla h_K^n \right\}_{\mathbf{k}},$$

where $|\mathbf{k}| = \sqrt{k_1^2 + k_2^2}$ is the magnitude of $\mathbf{k}$ and $\{f\}_{\mathbf{k}}$ represents the $\mathbf{k}$th-mode Fourier coefficient of the function f. The Fourier coefficients of the nonlinear term $(1 - |\nabla h_K^n|^2 + A)\nabla h_K^n$ are calculated by performing the discrete fast Fourier transform (FFT). It is readily seen that for a given level n the evaluation of all $\{(1 - |\nabla h_K^n|^2 + A)\nabla h_K^n\}_{\mathbf{k}}$ requires $8N$ one-dimensional FFT with vector length $N = 2K$. This is also the total cost to compute $\hat{h}_{\mathbf{k}}^{n+1}$ from (4.5). In practical calculation, we work on the spectral space. At the final time level, an additional FFT is needed to recover the physical nodal values $h_K^{n+1}(\mathbf{x})$ from $\hat{h}_{\mathbf{k}}^{n+1}$, $-K \leq k_1, k_2 \leq K$.

The purpose of this section is to verify the stability of the proposed numerical schemes in terms of the choice of the constant A. More serious applications will be reported in the next section.

Example 4.1. Consider an isotropic symmetry current model (2.1):

$$(4.6) \qquad \begin{cases} h_t = -\delta\Delta^2 h - \nabla \cdot [(1 - |\nabla h|^2)\nabla h], & [0, 2\pi]^2 \times (0, T], \\ h(\cdot, t) \ is \ 2\pi - \text{periodic} & \forall t \in (0, T], \\ h(\mathbf{x}, 0) = h_0(\mathbf{x}) & \forall \mathbf{x} \in [0, 2\pi]^2 \end{cases}$$

with $\delta = 0.1, 0.01, 0.001$ and

$$(4.7) \qquad h_0(\mathbf{x}) = 0.1(\sin 3x \sin 2y + \sin 5x \sin 5y).$$

This problem was used by Li and Liu [12] to study the most unstable modes. It was proved that with the initial condition (4.7) the most unstable modes are those with wave-vectors $\mathbf{k}$ such that $|\mathbf{k}| = \sqrt{5}$. Numerically, they showed that after short interaction of the unstable modes, the solution converges to a *steady state* which consists mainly of one mode only.

Define Δt_c as the largest possible time which allows stable numerical computation. In other words, if the time step is greater than Δt_c, then the numerical solution will blow up. In Table 1, we list the values of Δt_c for the schemes (2.4), (3.1), and (3.15) with different choices of A. All these semidiscrete schemes are approximated by the Fourier spectral methods in space. The Fourier mode number used in the calculations is $K = 128$. Several observations are made from Table 1:

- If $A = 0$, i.e., if a conventional implicit-explicit approach is used, then the numerical methods suffer from extremely small time steps, in particular when higher-order schemes are used or $\delta \ll 1$.
- The improvement on stability with the use of the constant A is significant. When A is sufficiently large (in this case $A \geq 2$), quite large time steps (in this case $\Delta t \geq 1$) can be used for first- and second-order time discretizations.

TABLE 1
Example 4.1: *stability comparison with different A and δ. Here* BDr *stands for rth-order backward differentiation and* EPr *for rth-order extrapolation.*

δ	A	BD1/EP1	BD2/EP2	BD3/EP3
0.1	$A = 0$	$\Delta t_c \approx 1$	$\Delta t_c < 0.3$	$\Delta t_c < 0.1$
	$A = 1$	$\Delta t_c \approx 1$	$\Delta t_c \approx 1$	$\Delta t_c \approx 0.5$
	$A = 2$	$\Delta t_c \approx 1$	$\Delta t_c \approx 1$	$0.2 \leq \Delta t_c < 0.5$
0.01	$A = 0$	$\Delta t_c < 0.1$	$\Delta t_c < 0.01$	$\Delta t_c < 0.002$
	$A = 1$	$\Delta t_c \approx 1$	$\Delta t_c \approx 0.1$	$\Delta t_c \approx 0.002$
	$A = 2$	$\Delta t_c \approx 1$	$\Delta t_c \approx 1$	$\Delta t_c \approx 0.05$
0.001	$A = 0$	$\Delta t_c < 0.01$	$\Delta t_c < 0.001$	$\Delta t_c < 10^{-4}$
	$A = 1$	$\Delta t_c \approx 1$	$\Delta t_c \approx 0.005$	$0.0005 \leq \Delta t_c < 10^{-3}$
	$A = 2$	$\Delta t_c \approx 1$	$\Delta t_c \approx 1$	$\Delta t_c \approx 0.005$

• The choice of A depends on the order of time discretization. For the third-order methods, a quite small time step has to be used, which is impractical for large time simulations.

We now turn to time accuracy comparison. Since the exact solution for problem (4.6) is unknown, we use numerical results of BD3/EP3 with $\Delta t = 0.0001$ and $K = 128$ as the "exact" solution. The coefficient δ is set to be 0.01 and the numerical errors are computed at $t = 1$. In this case, the "exact" solution obtained by using BD3/EP3 is plotted in Figure 1. Table 2 shows the L^2-errors using several values of A and
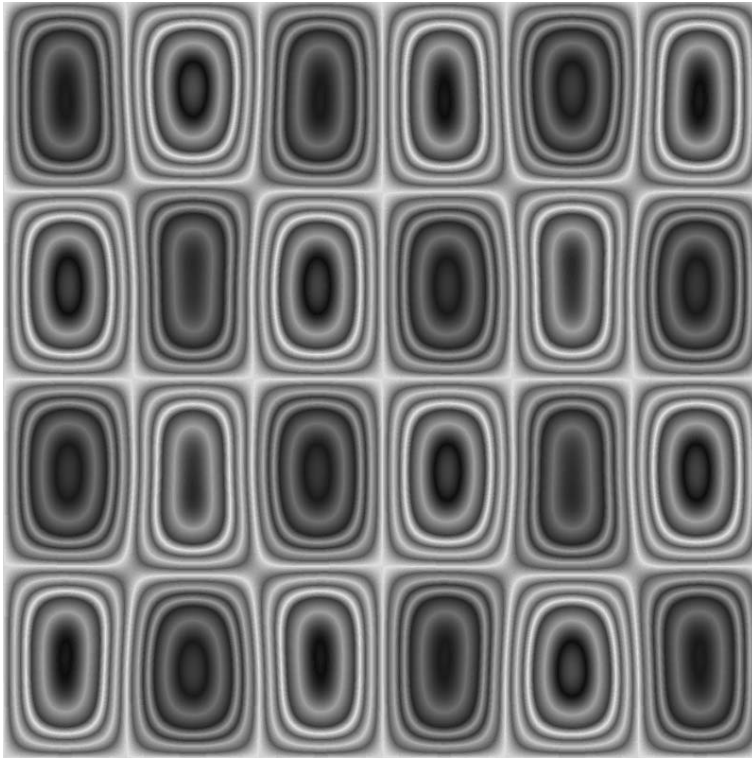

FIG. 1. *Isolines of the solution at $t = 1$ for $\delta = 0.01$.*

TABLE 2
Example 4.1: *accuracy with different choices of A.* $\delta = 0.01$.

A	Δt	BD1/EP1	BD2/EP2	BD3/EP3
$A = 0$	$\Delta t = 0.01$	0.72E-03	unstable	unstable
	$\Delta t = 0.005$	0.36E-03	0.24E-04	unstable
	$\Delta t = 0.0025$	0.18E-03	0.61E-05	unstable
	$\Delta t = 0.00125$	0.90E-04	0.16E-05	unstable
$A = 1$	$\Delta t = 0.01$	0.22E-02	0.21E-03	unstable
	$\Delta t = 0.005$	0.11E-02	0.56E-04	unstable
	$\Delta t = 0.0025$	0.51E-03	0.14E-04	unstable
	$\Delta t = 0.00125$	0.25E-03	0.37E-05	0.43E-06
$A = 2$	$\Delta t = 0.01$	0.43E-02	0.32E-03	0.22E-03
	$\Delta t = 0.005$	0.19E-02	0.87E-04	0.21E-04
	$\Delta t = 0.0025$	0.88E-03	0.23E-04	0.30E-05
	$\Delta t = 0.00125$	0.43E-03	0.58E-05	0.53E-06

four time steps. It is seen that once the methods are stable, the expected order of convergence (in time) is obtained.

5. Numerical experiments: Coarsening dynamics. In this section, we present the numerical results by simulating the MBE model (1.1) in cases of both isotropic surface (2.1) and square surface (2.2). The simulations are carried out in the domain $\Omega = (0, 1000)^2$, where double periodic boundary conditions are used in the spatial directions. The initial condition is a random state by assigning a random number varying from -0.001 to 0.001 to each grid point. The second-order schemes, i.e., (3.1) for the isotropic surface model and (3.14) for the square surface model, are used in our simulations. The spatial discretization is based on a Fourier pseudospectral approximation with K denoting the Fourier mode number. In order to investigate the effect of the time and space resolution, different values of Δt and K have been tested.

5.1. Growth on the isotropic symmetry surfaces. First we carry out the simulation of the growth process for the case of isotropic surfaces. In Figures 2 and 3, the isolines of the free energy $F_{free}(\mathbf{x}, t)$ at $t = 40,000$ and $80,000$ are plotted, respectively, with $(K, \Delta t) = (512, 1)$ and $A = 1$, where $F_{free}(\mathbf{x}, t)$ is defined by

$$F_{free} = \frac{1}{4}(|\nabla h|^2 - 1)^2 + \frac{\delta}{2}|\Delta h|^2.$$

The contourlines of F_{free} are usually used to identify the edges of the pyramidal structures since the free energy is concentrated on the edges. In these two figures the temporal evolution of the morphology of the growing surface is well visualized. It is seen that the edges of the pyramids (white areas) form a random network over the surface and separate the facets of the pyramids. The pyramids grow in time via a coarsening process, as is evident from Figures 2 and 3. Also shown is the randomness of the orientation of the pyramid edges, resulting from the isotropic nature of the surface symmetry. This result is in good agreement with the published results; see, e.g., [14].

Figure 4 presents the power laws of the growth of the interface height $\tilde{h}(t)$ and width $\lambda(t)$ of the pyramidal structures. Here $\tilde{h}(t)$ is defined by

$$\tilde{h}(t) = \left(\frac{1}{|\Omega|} \int_{\Omega} h^2(\mathbf{x}, t) d\mathbf{x} \right)^{\frac{1}{2}}.$$
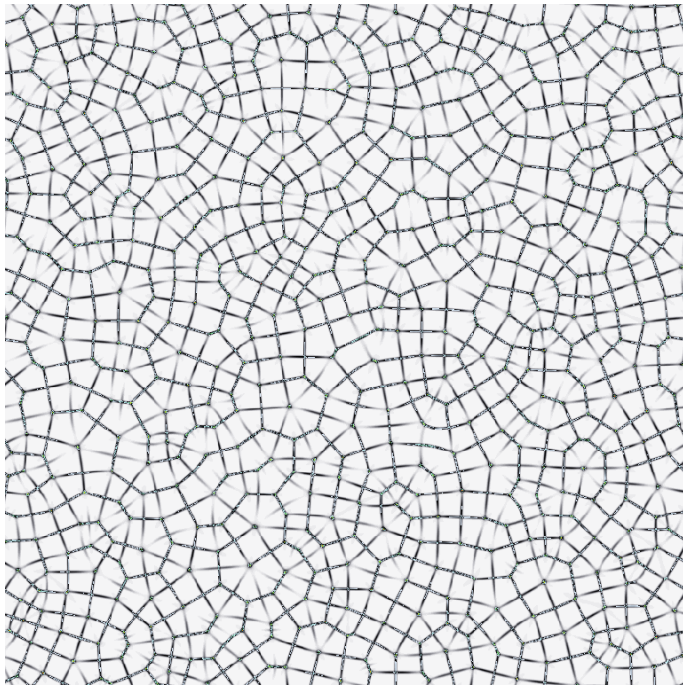
FIG. 2. *The isotropic symmetry surfaces problem: the contour plot at $t = 40{,}000$, obtained by using $K = 512$ and $\Delta t = 1$.*
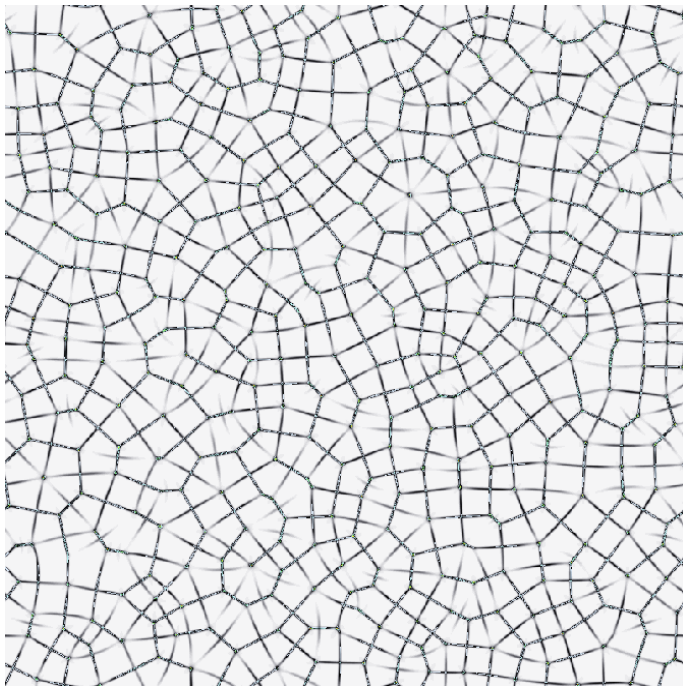

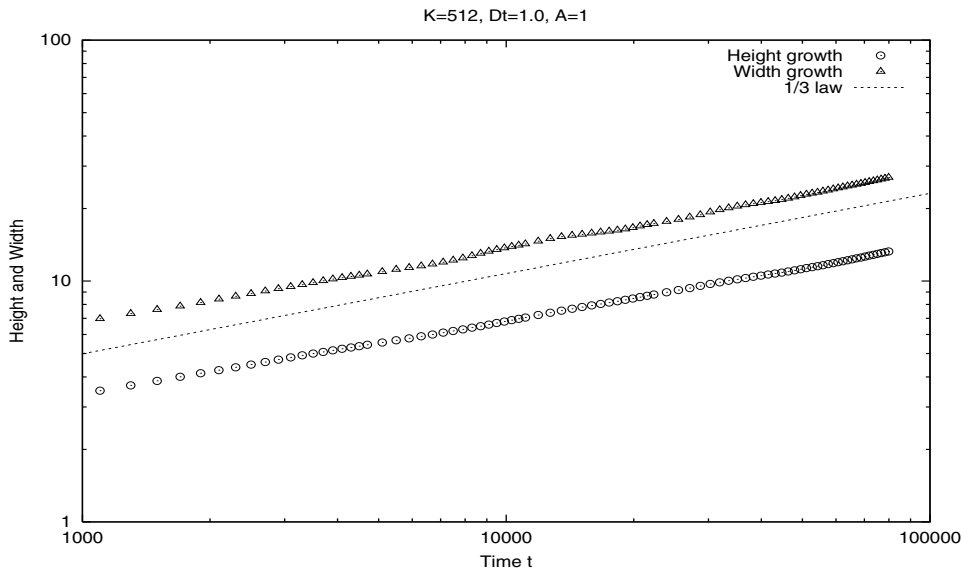FIG. 3. *Same as Figure* 2, *except at $t = 80{,}000$.*

Fig. 4. *The isotropic symmetry surfaces problem: growth power law obtained by using $K = 512$ and $\Delta t = 1$ (log-to-log scale).*

The width of the pyramid edges $\lambda(t)$ measures the mean size of the network cell, which can be calculated as in [14] from the height-height correlation function

$$K_{hh}(\mathbf{r}, t) = \int_\Omega h(\mathbf{x} + \mathbf{r}, t) h(\mathbf{x}, t) d\mathbf{x},$$

where $\mathbf{r}$ is a positive vector. In our calculations, we used a simpler form $\mathbf{r} = (r, r)^T$. With $\mathbf{r} = (r, r)^T$, $K_{hh}(\mathbf{r}, t)$ can be considered as a function of r for fixed t, and shows an oscillatory character reflecting the presence of mound structures. For a given t, the mean pyramid width $\lambda(t)$ is defined as $r_0(t)$, which is the first zero crossing of $K_{hh}(\mathbf{r}, t)$,

$$r_0(t) = \inf\{r > 0, K_{hh}(\mathbf{r}, t) = 0\}.$$

We see from Figure 4 that both vertical height and lateral width of the pyramids grow in time as power law ct^n with exponents n close to $\frac{1}{3}$ (slope of the lines), which is again in good agreement with the existing experimental and numerical results [14, 23].

In order to check the temporal and spatial resolution, we display in Figure 5 the result obtained by using $(K, \Delta t) = (256, 0.5)$, i.e., halving the values of K and Δt. It is observed from Figures 4 and 5 that there is no significant difference between the results obtained by using the two sets of parameters.

To demonstrate the robustness of the proposed method, we plot in Figure 6 the evolution of the mean height

$$\bar{h}(t) = \frac{1}{|\Omega|} \int_\Omega h(\mathbf{x}, t) d\mathbf{x}.$$

It is observed that $\bar{h}(t)$ remains practically zero in the entire time intervals. This demonstrates the mass conservation which can be derived from (2.1). The energy defined in (2.7), normalized by the domain size, is plotted in Figure 7. The decay of the energy as observed in Figure 7 agrees with the theoretical result (2.6).
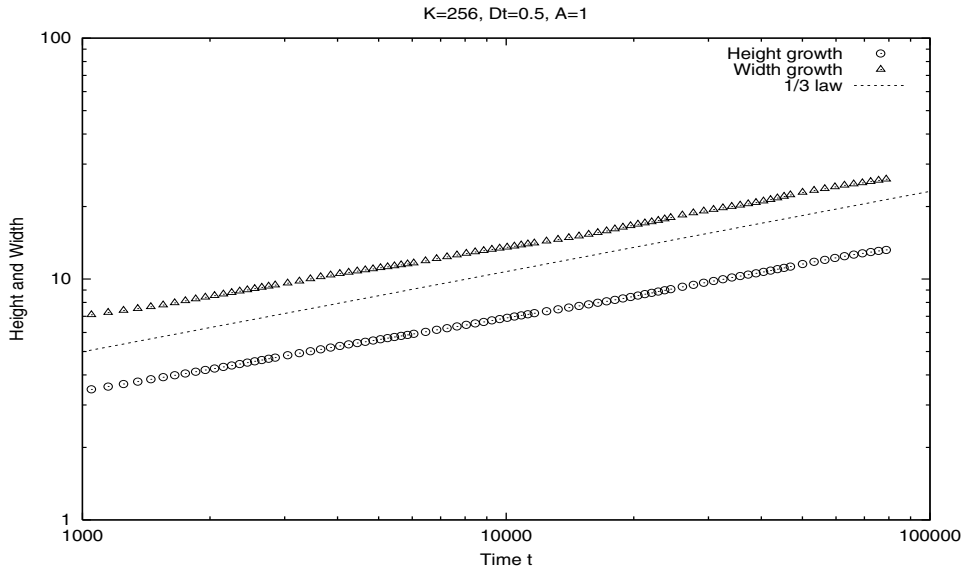
FIG. 5. *Same as Figure 4, except with $K = 256$ and $\Delta t = 0.5$.*
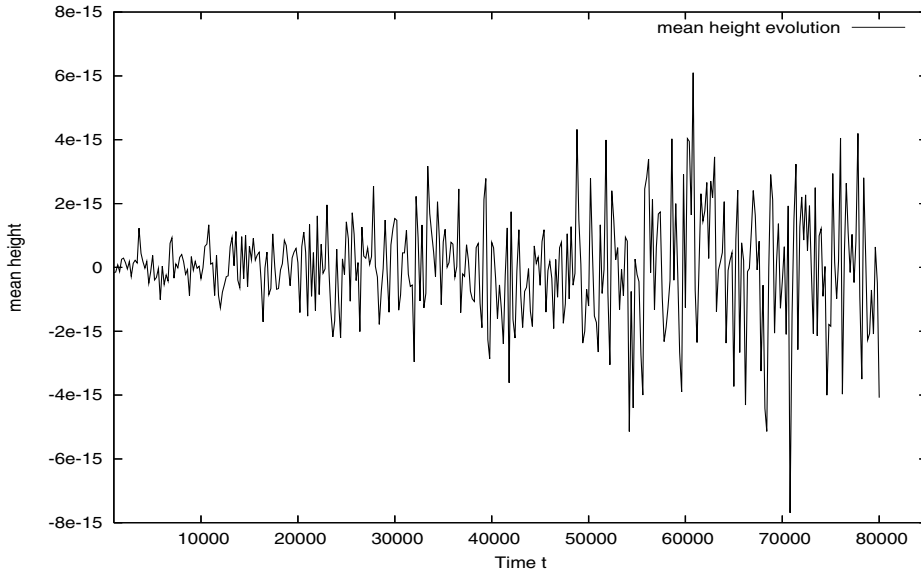

FIG. 6. *Evolution of the mean height as a function of the time.*

5.2. Growth on the square symmetry surfaces. Here we present simulation results obtained by solving the MBE model (2.2). The time discretization used in the simulation is the second-order scheme (3.14), and the space discretization is the same as in the isotropic case but here with Fourier mode number $K = 384$ and time step $\Delta t = 0.2$.
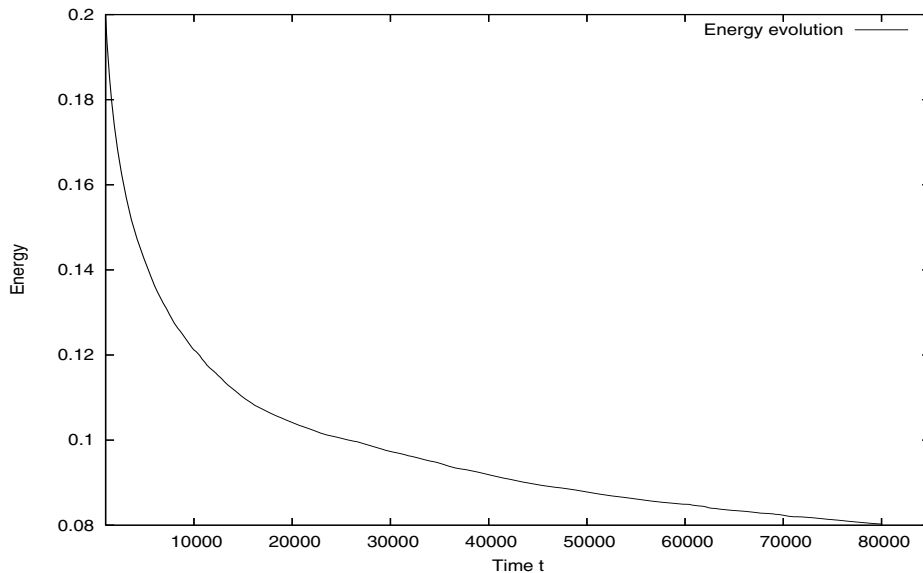
FIG. 7. *Evolution of the energy as a function of the time.*

In Figures 8 and 9, we plot the contourlines of the free energy function F'_{free} corresponding to the square symmetry model,

$$F'_{free} = \frac{\delta}{2}|\Delta h|^2 + \frac{1}{4}\left[(h_x^2 - 1)^2 + (h_y^2 - 1)^2\right].$$

As in the case of the isotropic surfaces, pyramid-like structures are growing in the surface with sharp edges carrying most of the energy, identified by the network formed by the white areas. However, in contrast to the isotropic case, the pyramid edges are well oriented toward the four preferred directions reflecting the square symmetry. A careful look at the two figures finds that the well-known dislocation feature is also presented, as reported by many experiments and simulations. Moreover, it is observed from Figure 10 that the power law obtained for the pyramid growth with the square symmetry is close to $\frac{1}{4}$. This is in good agreement with the numerical predictions of Siegert [19] and Moldovan and Golubovic [14].

6. Conclusions. In this work, we have developed and analyzed stable numerical methods for a class of nonlinear diffusion equations modeling epitaxial growth of thin films. Here, stability means that the decay of energy is preserved. In particular, we analyzed the stability properties of a class of semidiscretized (in time) schemes which are designed for large-system and long-time simulations. It is demonstrated that the classical semi-implicit method can be improved by simply adding some linear terms consistent with the truncation errors in time. The linear term consists of mixed derivatives, and the resulting numerical schemes are still semi-implicit with explicit treatment for the nonlinear terms. We also performed numerical simulations using the proposed schemes in time coupled with a Fourier spectral method in space for the molecular beam epitaxy model and determined power laws for the coarsening process. The numerical results are in good agreement with the existing ones, e.g., Moldovan and Golubovic [14] who directly solved a so-called type-A dynamics equation on a hexagonal grid.
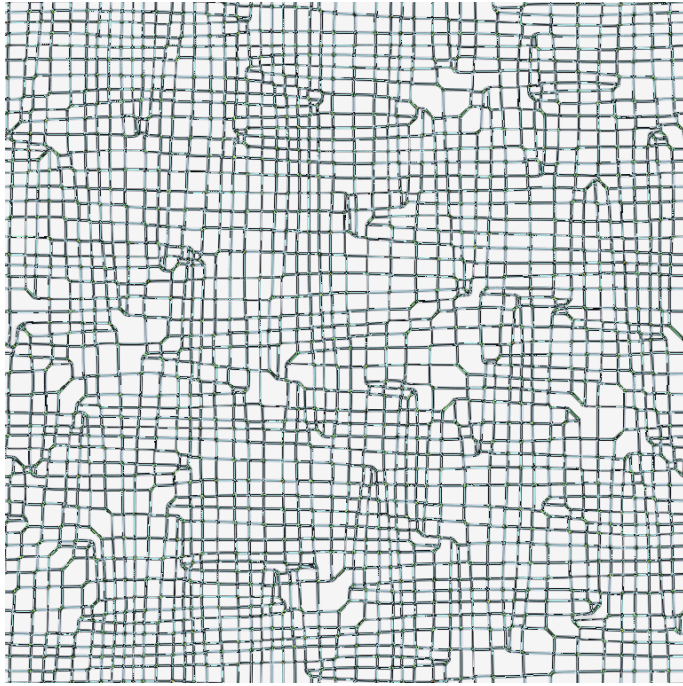
FIG. 8. *The square symmetry surface problem: the contour plot at $t = 40,000$, obtained by using $K = 384$ and $\Delta t = 0.2$.*
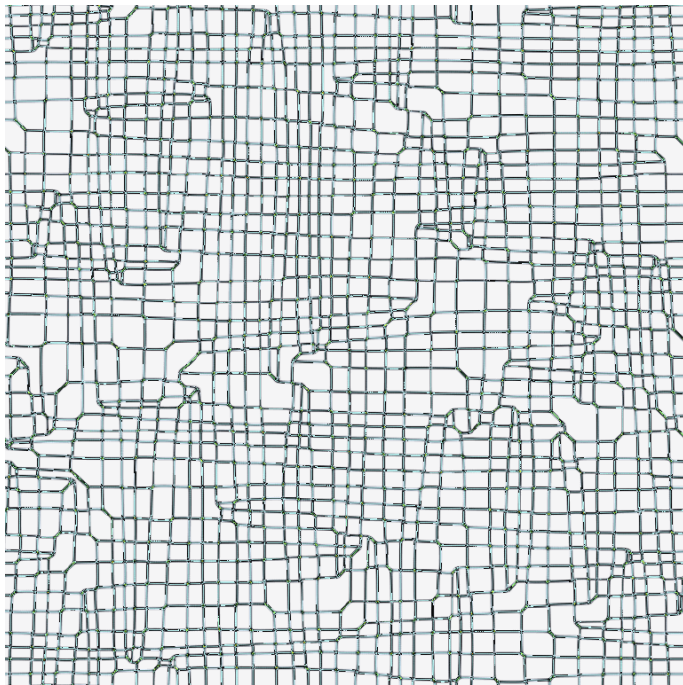

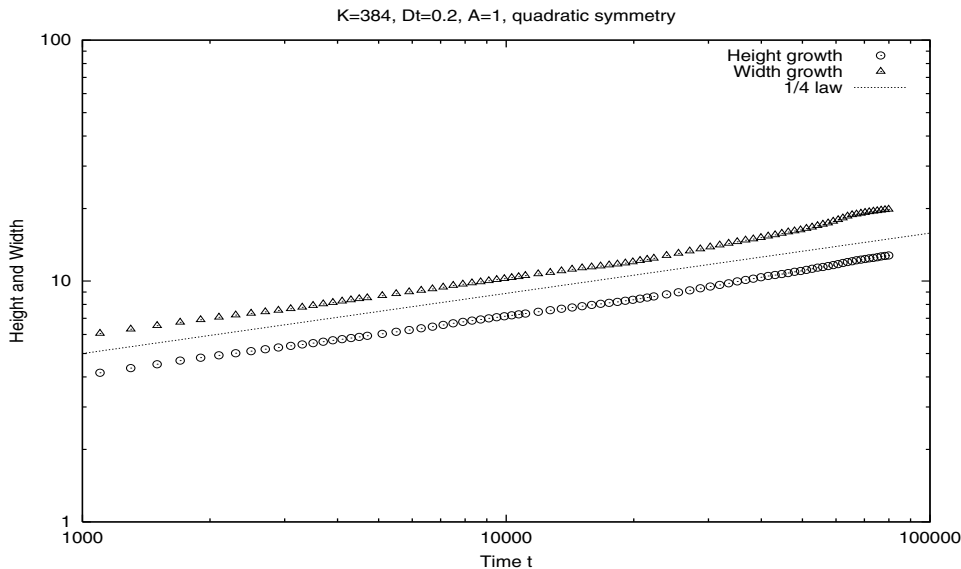FIG. 9. *Same as Figure* 8, *except at $t = 80,000$.*

Fig. 10. *The square symmetry surface problem: growth power law obtained by using $K = 384$ and $\Delta t = 0.2$.*

One of the future works in this direction is to carry out more rigorous analysis for the large time-stepping techniques, including stability analysis for higher-order schemes (say, third-order time-stepping) and error analysis for the proposed schemes. Obtaining a satisfactory error bound for a numerical scheme for the MBE models seems difficult: A direct error analysis shows that the error bounds are dependent on the surface diffusion constant δ and the solution time interval, which leads to unacceptable estimates for small δ and large T. A desired bound should have weak dependence on δ and T, which seems very difficult. Other future works in this direction include adaptive time integration, i.e., treating the fast dynamics changes and slow changes separately. This is also important in improving the efficiency for the large-time simulations.

REFERENCES

[1] A.-L. BARABÁSI AND H. E. STANLEY, *Fractal Concepts in Surface Growth*, Cambridge University Press, Cambridge, UK, 1995.
[2] J. P. BOYD, *Chebyshev and Fourier Spectral Methods*, 2nd ed., Dover, Mineola, NY, 2001.
[3] R. E. CAFLISCH, M. F. GYURE, B. MERRIMAN, S. OSHER, C. RATSCH, D. D. VVEDENSKY, AND J. J. ZINCK, *Island dynamics and the level set method for epitaxial growth*, Appl. Math. Lett., 12 (1999), pp. 13–22.
[4] S. CLARKE AND D. D. VVEDENSKY, *Origin of reflection high-energy electron-diffraction intensity oscillations during molecular-beam epitaxy: A computational modeling approach*, Phys. Rev. Lett., 58 (1987), pp. 2235–2238.
[5] B. COSTA, W.-S. DON, D. GOTTLIEB, AND R. SENDERSKY, *Two-dimensional multi-domain hybrid spectral-WENO methods for conservation laws*, Commun. Comput. Phys., 1 (2006), pp. 550–577.

[6] G. Ehrlich and F. G. Hudda, *Atomic view of surface diffusion: Tungsten on tungsten*, J. Chem. Phys., 44 (1966), pp. 1039–1049.

[7] X. B. Feng and A. Prohl, *Error analysis of a mixed finite element method for the Cahn-Hilliard equation*, Numer. Math., 99 (2004), pp. 47–84.

[8] M. F. Gyure, C. Ratsch, B. Merriman, R. E. Caflisch, S. Osher, J. J. Zinck, and D. D. Vvedensky, *Level-set methods for the simulation of epitaxial phenomena*, Phys. Rev. E (3), 58 (1998), pp. 6927–6930.

[9] H. C. Kang and W. H. Weinberg, *Dynamic Monte Carlo with a proper energy barrier: Surface diffusion and two-dimensional domain ordering*, J. Chem. Phys., 90 (1989), pp. 2824–2830.

[10] R. V. Kohn and X. Yan, *Upper bounds on the coarsening rate for an epitaxial growth model*, Comm. Pure Appl. Math., 56 (2003), pp. 1549–1564.

[11] J. Krug, *Origins of scale invariance in growth processes*, Adv. in Phys., 46 (1997), pp. 139–282.

[12] B. Li and J. G. Liu, *Thin film epitaxy with or without slope selection*, European J. Appl. Math., 14 (2003), pp. 713–743.

[13] B. Li and J. G. Liu, *Epitaxial growth without slope selection: Energetics, coarsening, and dynamic scaling*, J. Nonlinear Sci., 14 (2004), pp. 429–451.

[14] D. Moldovan and L. Golubovic, *Interfacial coarsening dynamics in epitaxial growth with slope selection*, Phys. Rev. E (3), 61 (2000), pp. 6190–6214.

[15] M. Ortiz, E. Repetto, and H. Si, *A continuum model of kinetic roughening and coarsening in thin films*, J. Mech. Phys. Solids, 47 (1999), pp. 697–730.

[16] A. Pimpinelli and J. Villain, *Physics of Crystal Growth*, Cambridge University Press, Cambridge, UK, 1998.

[17] M. Schneider, I. K. Schuller, and A. Rahman, *Epitaxial growth of silicon: A molecular-dynamics simulation*, Phys. Rev. B, 36 (1987), pp. 1340–1343.

[18] R. L. Schwoebel and E. J. Shipsey, *Step motion on crystal surfaces*, J. Appl. Phys., 37 (1966), pp. 3682–3686.

[19] M. Siegert, *Ordering dynamics of surfaces in molecular beam epitaxy*, Phys. A, 239 (1997), pp. 420–427.

[20] M. Siegert and M. Plischke, *Slope selection and coarsening in molecular beam epitaxy*, Phys. Rev. Lett., 73 (1994), pp. 1517–1520.

[21] E. Tadmor, *Super-viscosity and spectral approximations of nonlinear conservation laws*, in Numerical Methods for Fluid Dynamics IV, M. J. Baines and K. W. Morton, eds., Oxford University Press, New York, 1993, pp. 69–81.

[22] J. Y. Tsao, *Materials Fundamentals of Molecular Beam Epitaxy*, World-Scientific, Singapore, 1993.

[23] F. Tsui, J. Wellman, C. Uher, and R. Clark, *Morphology transition and layer-by-layer growth of Rh*(111), Phys. Rev. Lett., 76 (1996), pp. 3164–3167.

[24] J. Villain, *Continuum models of critical growth from atomic beams with and without desorption*, J. Phys. I, 1 (1991), pp. 19–42.

[25] D. Xiu and J. Shen, *An efficient spectral method for acoustic scattering from rough surfaces*, Commun. Comput. Phys., to appear.

[26] J. Zhu, L.-Q. Chen, J. Shen, and V. Tikare, *Coarsening kinetics from a variable-mobility Cahn-Hilliard equation: Application of a semi-implicit Fourier spectral method*, Phys. Rev. E (3), 60 (1999), pp. 3564–3572.